JCTC Journal of Chemical Theory and Computation

Article

pubs.acs.org/JCTC

Generation of Well-Relaxed All-Atom Models of Large Molecular Weight Polymer Melts: A Hybrid Particle-Continuum Approach Based on Particle-Field Molecular Dynamics Simulations

Antonio De Nicola,[†,‡] Toshihiro Kawakatsu,[§] and Giuseppe Milano*[,†,‡]

[†]Dipartimento di Chimica e Biologia, Università degli Studi di Salerno, via Ponte don Melillo, Fisciano, Salerno I-84085, Italy

[‡]IMAST Scarl-Technological District in Polymer and Composite Engineering, Piazza Bovio 22, Napoli, Napoli I-80133, Italy

[§]Department of Physics, Tohoku University, Aoba, Aramaki, Aoba-ku, Sendai, Miyagi 980-8578, Japan

Supporting Information

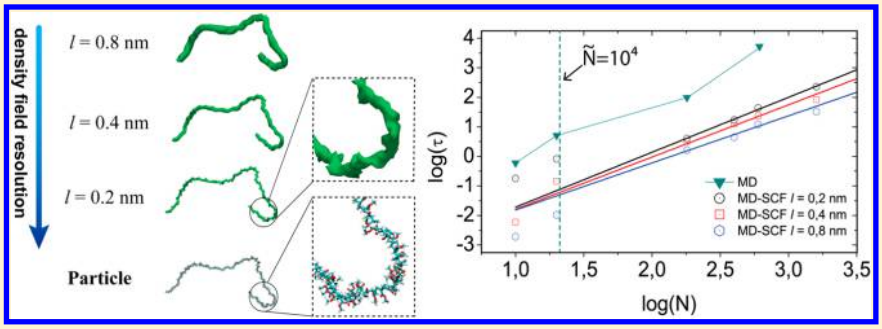

ABSTRACT: A procedure based on Molecular Dynamics (MD) simulations employing soft potentials derived from self-consistent field (SCF) theory (named MD-SCF) able to generate well-relaxed all-atom structures of polymer melts is proposed. All-atom structures having structural correlations indistinguishable from ones obtained by long MD relaxations have been obtained for poly(methyl methacrylate) (PMMA) and poly(ethylene oxide) (PEO) melts. The proposed procedure leads to computational costs mainly related on system size rather than to the chain length. Several advantages of the proposed procedure over current coarse-graining/reverse mapping strategies are apparent. No parametrization is needed to generate relaxed structures of different polymers at different scales or resolutions. There is no need for special algorithms or back-mapping schemes to change the resolution of the models. This characteristic makes the procedure general and its extension to other polymer architectures straightforward. A similar procedure can be easily extended to the generation of all-atom structures of block copolymer melts and polymer nanocomposites.

1. INTRODUCTION

The behavior of synthetic polymers has been thoroughly investigated based on simple and idealized models within the framework of the seminal works of Flory[1,2] and de Gennes.[3] According to the picture resulting from these studies, all polymers with a specified branching structure, although they have different chemistries, follow universal scaling laws when they are in a melt or dissolved in a solvent of the same quality, and these scaling features allow us to understand polymers' behavior qualitatively. In conjunction with these theories, specific models of synthetic polymers have remained very useful in predicting and understanding the relationship between chemical structures and the key physical and chemical properties of polymeric materials. For this reason, the development of predictive computational schemes able to model the details of atomistic structures and evaluate their relationship with final properties has been a subject of intensive study.[4−7] To this end, due to the increasing development of computer performance, simulation techniques have become important tools of research in polymer science. In particular, molecular dynamics techniques have been employed to study different aspects of polymeric materials.[8−15]

Macromolecules, even single chains thereof, exhibit much more complex behavior than simple molecular liquids do, and the main difficulties associated with simulating polymers are related to the intrinsically multiscale nature of macromolecules. In fact, macromolecules' structure gives rise to a wide range of coupled length and time scales. Scales of several orders of magnitude are strongly connected for a single chain, in which the typical length scales range from the scale of a single chemical bond (order of 1 Å) to that of the persistence length (∼1 nm) and finally to that of the radius of gyration of the chain (∼10 nm). The range becomes even broader if packing of different chains is considered. In particular, from the local packing of chains in the bulk (on the order of atomic radii) to the smallest phase structures (lamellae, cylinders, spheres) in microphase-separated block copolymer systems (on the order

Received: June 6, 2014
Published: October 24, 2014

   dx.doi.org/10.1021/ct500492h | J. Chem. Theory Comput. 2014, 10, 5651−5667

Scheme 1. (A) Vertical Approach[a] and (B) Horizontal Approach[b]

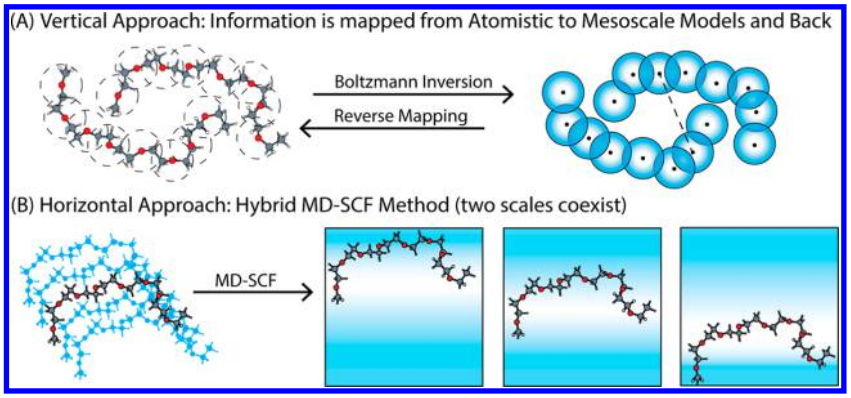

[a]The coarse-graining procedure involves particle reduction and information transferred from the atomistic level to a CG model and back. The two objects, atoms and beads, although connected by mapping and reverse-mapping procedures, do not coexist in the same model. [b]In this approach, unlike in the vertical approach, two scales of particles and fields coexist.

of 10 nm) or to the crystallites of semicrystalline polymers and domains in immiscible polymer blends (both on the order of μm), scales of several orders of magnitude are connected. A similar multiplicity of time scales is involved in the description of polymer dynamics. One of the fundamental aspects of polymer dynamics is chain entanglement. Referring to the situation in which macromolecules interpenetrate, the term entanglement describes the interactions arising from the uncrossability of chains.[16,17] In polymer melts and rubbers, these interactions determine dynamical, flow, and deformation properties.[3,17]

With the foregoing discussion in mind, modeling the structure−property relations of polymeric materials at the atomic level involves the preparation of equilibrated melts of long, entangled chains. Melts consisting of oligomers can be equilibrated by sufficiently long molecular dynamics or Monte Carlo simulations. By contrast, high molecular weight polymer chains are very difficult to treat because they are difficult to relax. In fact, for chains longer than the entanglement length, the dynamics is dramatically slowed down.[18] To understand the level of computational effort required for polymer simulations, the longest relaxation process of an entangled polymer melt of length N scales at least as N^3, which corresponds to at least N^4 in CPU time, and the computer time required for reliable equilibration is out of reach, especially for large systems.

Thus, coarse-graining methods for simulating polymer behavior have been widely utilized to solve this problem.[19−26] The general strategy involves a reduction of the number of degrees of freedom by simplifying the models used and retaining only those degrees of freedom that are relevant for a particular range of interest. In practice, several atoms are grouped together into "super-atoms". The potentials between superatoms are adjusted to reproduce mainly the structural properties of a polymer. Following this approach, different polymer properties have been calculated by mesoscale simulations, yielding results that are in good agreement with experimental data for polymer melts,[21−24,27,28] blends,[29] and composites.[30] In the same spirit, the multiscale coarse-graining approach introduced by Izvekov and Voth[31,32] uses a variational procedure to build effective coarse-grained (CG) interactions from atomistic reference simulations. The use of these or similar approaches involving several specific coarse-grained models is currently proposed for different synthetic polymer architectures. For example, models have very recently been reported for methacrylates,[33] atactic polystyrene,[34] polybutadiene melts,[35] Pluronics in contact with biomembranes[36] and in water solutions,[37] and coarse-grain solvent molecules for biopolymers.[38]

In all of the aforementioned cases, the model setup is related to the chemical structure of the repeating unit. Thus, it is possible to reintroduce, after global relaxation of the system, the chemical details of the chains. The combination of CG simulation with an efficient back-mapping methodology (i.e., reintroduction of atomistic detail) is a strategy for circumventing the time scale problem and for obtaining well-equilibrated atomistic structures. In fact, state-of-the-art atomistic modeling of high molecular weight polymer chains involves a complicated procedure of atomistic simulations → derivation of a coarse-grained model; coarse-grained simulations → reverse-mapping and local relaxation of the atomistic model (see Scheme 1, vertical approach).[19,27,39−45] In this vein, a hierarchical procedure using sequential back-mapping from coarse-grained configurations was recently proposed by Kremer and co-workers.[46]

On the other hand, a coarse-graining approach based on particle continuum bridging has been proposed more recently. In particular, molecular models can be developed in a hybrid particle-field scheme combining particles with a field representation employed for the calculation of nonbonded interactions. The use of density fields in off-lattice MC simulations has been originally introduced by Laradji et al.[47] to study the equilibrium properties of polymer brushes. Nowadays, due to their computational efficiency, hybrid models are gaining popularity (for recent reviews, the reader can refer to refs 48−50). The combination of particle and field representations has been recently considered for single chains in the mean-field method reported by Daoulas, Mueller, and co-workers[51,52] and applied to Monte Carlo (MC) simulations of CG models of homopolymer and block copolymers.[53,54] Several CG models using a hybrid representation of polymer melts, polymer nanocomposites, biocompatible polymers,[44] biomembranes,[44,50,55−58] and vescicles[59] have been reported. In this framework, more recently, the molecular dynamics (MD) technique has been combined with the self-consistent field (SCF) method, a technique which we hereafter refer to as the "MD-SCF" approach.[60,61] The peculiar feature of the MD-SCF approach is that the interactions among nonbonded particles are evaluated through an external potential dependent on the

dx.doi.org/10.1021/ct500492h | J. Chem. Theory Comput. 2014, 10, 5651−5667

local density. In this manner, the molecular motion in a many-molecule system is reduced to the derivation of a partition function of a single molecule in an external field. This approximation enables us to effectively exploit the parallelization of molecular dynamics simulations and to handle large-scale systems.[62]

The two coarse-graining approaches, the first based on particle reduction and the second based on a hybrid particle-field representation, are conceptually different. This difference is outlined graphically in Scheme 1. In particular, in the first case, the coarse-graining approach can be defined as vertical, in which information is mapped from an atomistic level (or from a less coarse representation) to a coarser level, and, in the reverse direction, the procedure usually depends on the particular chemical structure that needs to be defined.[22,39,42,43]

In the second case, the coarse-graining approach can be defined as horizontal, in which the particles and the field representations coexist in the same model. This conceptual difference leads to several practical and technical advantages of the hybrid particle-continuum approach that can be exploited in the generation of well-relaxed atomic structures of polymer melts.

In the present paper, we propose a procedure based on MD-SCF simulations that is able to generate well-relaxed all-atom structures of polymer melts. In section 2.1, a brief introduction to the simulation technique and hybrid particle-field models is presented. In sections 2.2 and 2.3, the details of the simulation and of the models are given. In section 2.4 the proposed relaxation procedure is described. In the discussion section, the procedure for obtaining well-relaxed structures is described in detail. Applications of this procedure to two polymer models, i.e., poly methyl-methacrylate (PMMA) and poly ethylene-oxide (PEO) (see Scheme 2), are reported. In particular, the structural and dynamic properties of the hybrid MD-SCF and classical models based on pairwise interactions (named MD in the following) are compared and discussed.

Scheme 2. Chemical Structures of Repeating Units of (A) PMMA and (B) PEO

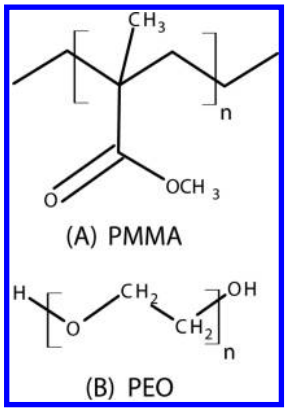

2.1. Method and Models. The all-atom models considered in this work were developed in a hybrid MD-SCF scheme combining particles with a field representation for nonbonded interactions. According to self-consistent field (SCF) theory, a particle is considered to interact with nonbonded particles only through a mean field. The derivation of such a mean-field representation is obtained by splitting the Hamiltonian of a system composed of M molecules into two parts:

$$\hat{H}(\Gamma) = \hat{H}_0(\Gamma) + \hat{W}(\Gamma) \tag{1}$$

In eq 1, Γ specifies a point in phase space and is used as a shorthand for a set of positions of all atoms in the system configuration. Moreover, in the following, the symbol $\hat{}$ (hat) indicates that the associated physical quantity is a function of the microscopic states corresponding to the phase space Γ. The term $\hat{H}_0(\Gamma)$ is the Hamiltonian of a reference system composed of molecules interacting only through the intramolecular bonding parameters (bond, angle, etc.) that are usually considered in MD simulations. The deviation from the reference system due to nonbonded interactions is denoted as $\hat{W}(\Gamma)$.

Assuming a canonical (NVT) ensemble, the partition function of the system is

$$Z = \frac{1}{M!}\int d\Gamma \exp\{-\beta[\hat{H}_0(\Gamma) + \hat{W}(\Gamma)]\} \tag{2}$$

where $\beta = 1/(k_B T)$.

The number density of particles, in microscopic fashion, can be defined as a sum of delta functions placed at the center of mass of each particle as follows[60]

$$\hat{\phi}(\mathbf{r};\Gamma) = \sum_{p=1}^{M}\sum_{i=0}^{S(p)} \delta(\mathbf{r} - \mathbf{r}_i^{(p)}) \tag{3}$$

where $S(p)$ indicates the number of particles belonging to the p-th molecule, and $\mathbf{r}_i^{(p)}$ is the position of the i-th particle in the p-th molecule.

The interaction term $\hat{W}(\Gamma)$ is calculated by introducing two main assumptions. The first assumption is that this interaction term depends on Γ but only through the particle number density $\hat{\phi}(\mathbf{r};\Gamma)$

$$\hat{W}(\Gamma) = W[\hat{\phi}(\mathbf{r};\Gamma)] \tag{4}$$

where the notation $W[\hat{\phi}(\mathbf{r};\Gamma)]$ indicates that W is a functional of $\hat{\phi}(\mathbf{r};\Gamma)$.

Equation 2 can be rewritten as a partition function of single molecules in an external field using an exact mathematical transformation (namely, Hubbard-Stratonovich transformation[63]).

The total nonbonded interaction energy of the system in the field approximation can be written as

$$W[\{\phi_K(\mathbf{r})\}] = \int d\mathbf{r}\left(\frac{k_B T}{2}\sum_{KK'}\chi_{KK'}\phi_K(\mathbf{r})\phi_{K'}(\mathbf{r}) + \frac{1}{2\kappa}\Big(\sum_K \phi_K(\mathbf{r}) - 1\Big)^2\right) \tag{5}$$

where $\phi_K(\mathrm{r})$ is the coarse-grained density of the species K at position r, and $\chi_{KK'}$ are mean-field parameters for the interaction of a particle of type K with the density fields due to particles of type K'. Here, $\phi_K(\mathrm{r})$ has been redefined as the number density of the species K normalized by the total average number density of the particles. More precisely, for each species K, $\phi_K(\mathbf{r})$ is a scaled number density $\phi_K(\mathbf{r}) = \rho_K(\mathbf{r})/\rho_0$, where $\rho_K(\mathbf{r})$ is the number density of the particles of type K at the position $\mathbf{r}$ and $\rho_0 = N/V$ (N is the total number of particles and V system volume). According to this definition the scaled density will be 1 at r if $\rho_K(\mathbf{r}) = \rho_0$. This modified definition of $\phi_K(\mathrm{r})$ only affects the scale of the conjugate field $V(\mathrm{r})$. The second term of the integrand on the right-hand side

dx.doi.org/10.1021/ct500492h | J. Chem. Theory Comput. 2014, 10, 5651−5667

of eq 5 is called the relaxed incompressibility condition, where κ is the compressibility that is assumed to be sufficiently small (for the systems considered in this paper, the value of $1/\kappa$ is 10 kJ/mol).[60] The second term of the integrand above is called relaxed incompressibility condition. Differently from classical MD nonbonded potentials, where excluded volume of atoms is accounted by a fast increase of repulsive part of Lennard-Jones potential, here excluded volume interactions are modeled through the incompressibility condition. In particular, the second term of the integrand above will be high (or low) if in some point of the space the density will be higher (or lower) than the average value. The introduction of the relaxed incompressibility condition keeps the total density constant and avoids accumulation of particles or voids. The value of κ fixes how stiff is the incompressibility condition and the fluctuations around the average value. In particular, for large values of kappa the incompressibility will be loose, and, on the contrary, for small values of kappa the condition will be stiff. Due to this analogy, κ was named "compressibility". The expression of the external potential $V(\mathbf{r})$ (see Supporting Information section S2) is found by replacing the integrals over $w(\mathbf{r})$ and $\varphi(\mathbf{r})$ of eq S14 with a Gaussian integral around the most probable state (saddle point approximation). In this framework, the mean field solution of eq S14, using saddle point approximation, is exactly in the limit $\tilde{N} \to \infty$ and is

$$V_K(\mathbf{r}) = \frac{\delta W[\{\phi_K(\mathbf{r})\}]}{\delta \phi_K(\mathbf{r})} = k_B T \sum_{K'} \chi_{KK'} \phi_{K'}(\mathbf{r}) + \frac{1}{\kappa}\left(\sum_K \phi_K(\mathbf{r}) - 1\right) \quad (6)$$

In the present study, which focuses on homopolymer melts, terms depending on $\chi_{KK'}$ are not considered; the only term included is the incompressibility condition. This assumption will be validated later. In this manner, the force acting on a particle at position $\mathbf{r}$ imposed by the interaction with the density field in the present case is

$$F(\mathbf{r}) = -\frac{\partial V(\mathbf{r})}{\partial \mathbf{r}} = -\frac{1}{\kappa}\left(\frac{\partial \phi(\mathbf{r})}{\partial \mathbf{r}}\right) \quad (7)$$

The sum over K in eq 7 is disregarded because we consider, in the field representation, all atom types as belonging to the same species.

From a computational point of view, the advantage of the hybrid MD-SCF scheme is that the most expensive part of the MD simulations, the calculation of the nonbonded forces, is replaced by the evaluation of forces between single particles with external potentials. For the calculation of these forces, it is necessary to obtain a smooth coarse-grained density function using the particle positions Γ. This procedure can be represented as follows

$$\overline{S}\{\hat{\phi}(\mathbf{r}; \Gamma)\} = \phi(\mathbf{r}) \quad (8)$$

where $\overline{S}$ denotes the mapping from particle positions to the coarse-grained density $\phi(\mathbf{r})$. In the current implementation, this density field is obtained by mapping particle positions on a density mesh. In particular, the simulation box is divided into several subcells. Then, according to the position of each particle inside a cell, a fraction of the particle is assigned to each vertex of the cell. To better visualize this procedure, a two-dimensional case is schematized in Figure 1A.

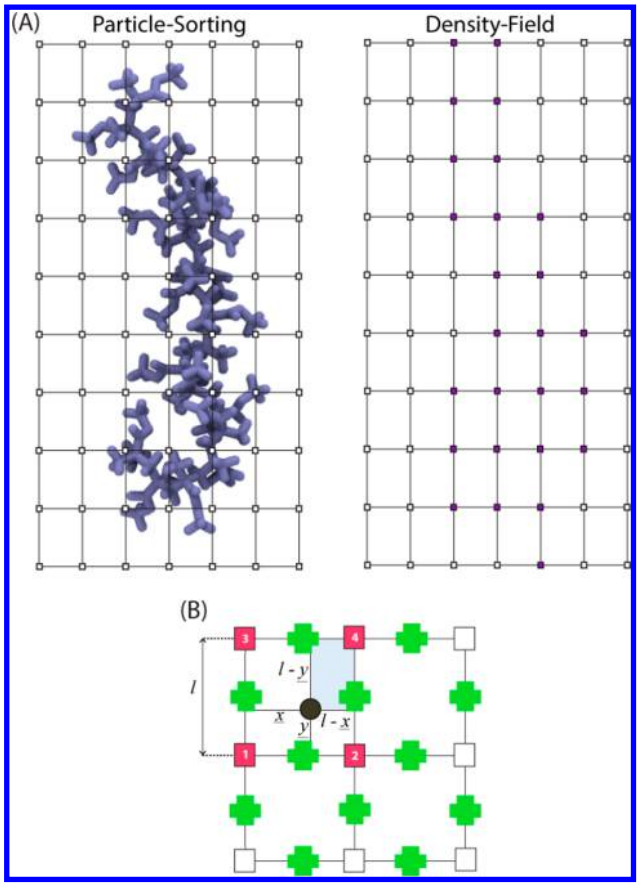

Figure 1. (A) An explanation, using a two-dimensional system, of the assignment of coarse-grained density to lattice points for a polymer chain (for clarity, the only backbone non-hydrogen atoms are shown). (B) Criterion for assignment of a particle fraction to lattice points. As schematized in the figure, the squares indicate the lattice points where the density is defined. Correspondingly, the density gradients, used for force calculations, are defined at the center of each edge (staggered lattice points indicated by crosses in part (B) of the square surrounding the density lattice points.

As shown in Figure 1B, the fraction of a particle assigned to a given lattice point is proportional to the area of the rectangles shown in the figure (in the actual 3-dimensional system, these are volumes of rectangular parallelepipeds). In particular, to point 1 in Figure 1B, a fraction of a particle proportional to the area (l-$x \times l$-y) of the filled rectangle will be assigned.

The size of the cell l is an important spatial parameter because it defines the extent to which the density is coarse-grained. In fact, if the value of l is large, many particles will be included in each cell, and the calculated density will become coarser. When the coarse-grained density is calculated from particle positions, the forces can be obtained from the spatial derivatives of the density fields.

The iteration scheme used in the MD-SCF approach is as follows: from the initial configuration of the system (at time t_0), a starting mesh representing the coarse-grained density is built, and density gradients at the particle positions are calculated by linear interpolation. Using the density gradients, the forces acting on the particles at position $\mathbf{r}$ due to the interaction with the density fields are computed according to eq 7. The total force on the particles is the sum of the intramolecular forces (bonds, angles, etc., calculated as in classical MD simulations) and the forces due to the interactions of particles with density

dx.doi.org/10.1021/ct500492h | J. Chem. Theory Comput. 2014, 10, 5651−5667

fields. It is important to stress that, for the proposed implementation, the use of mean fields does not correspond to a truly field-based method or simply particle−field coexistence. The density field is a close function of particle coordinates and is not an independent variable in the free energy functional. Furthermore, using the instantaneous field approximation introduced by Doulas et al. within the framework of a single chain in mean-field Monte Carlo simulations,[51] it is possible to tune a time interval to update the density field without loss of accuracy. The main assumption is that the field, as a collective variable, is characterized by a slow change with respect to particle displacements in one or more time steps. The choice of an optimal value of the updating frequency (Δt_{update}) depends on the resolution of the density (i.e., the size of the subcell in which the particles are grouped), the system properties, and the conditions applied. For the systems considered herein, it is observed that Δt_{update} values less than 1 ps yield sufficiently accurate results. According to this result, for all simulations reported in the paper, if different values are not explicitly mentioned, an update frequency of 0.1 ps has been used. This feature will be discussed in greater detail in the discussion section.

2.2. Atomistic Models Details. The force field for the full-atomistic PMMA model is obtained from refs 64 and 65, and the force field parameters for the PEO model are taken from refs 66 and 67. The functional forms and the bonding and nonbonding interaction parameters are reported in the Supporting Information (Section S1) for both the PMMA and PEO models.

The intramolecular interactions (bond and angle terms) of the hybrid models for PMMA and PEO employed in MD-SCF simulations are coincident with those reported in refs 65, 67, and 68, respectively.

2.3. Computational Details. Hybrid MD-SCF simulations were run in the *NVT* ensemble, in which the temperature was controlled using an Andersen thermostat[69] (collision frequency 7 ps^{-1}). Simulations were carried out at 500 K for PMMA and 343 K for PEO (see Table 1). A time step of 1 fs was employed in all simulations. The density field was updated using Δt_{update} = 0.1 ps, if not explicitely mentioned, in all MD-SCF simulations. Reference MD simulations were carried out in the *NVT* ensemble at the same temperatures employed for the MD-SCF simulations. The temperature was held constant with a Berendsen thermostat[70] (τ = 0.5 ps). A time step of 1 fs as used for both polymers. A cutoff distance of 1.0 nm was employed for both van der Waals and Coulomb interactions. The long-range corrections to electrostatic interactions were calculated using a reaction field[71] for PMMA, with a dielectric constant[72,73] ε = 2.6, and using the Ewald summation method[74] for PEO.

Table 1. Details of Simulated Systems

system	nr. chains	nr. units (*N*)	total nr. particles	nr. of backbone atoms	box length (nm)
PMMA-5[a]	60	5	4620	10	3.63
PMMA-10[a]	30	10	4560	20	3.68
PMMA-20[a]	15	20	4530	40	3.65
PMMA-180[a]	3	180	8106	360	4.45
PMMA-180B[a]	100	180	270200	360	14.3
PMMA-400[a]	3	400	12004	800	4.95
PMMA-600[a]	3	600	27006	1200	6.50
PMMA-1200[a]	3	1600	96008	3800	10.5
PEO-30[b]	27	30	5886	90	3.77

[a]PMMA melts were simulated at 500 K. [b]PEO melt were simulated at 343 K.

2.4. Relaxation Procedure. The general strategy described in detail and validated in the next section involves an increase in the model resolution to equilibrate stepwise systems from larger to smaller length scales and to recover an increasing number of features from a large length scale to a smaller one using reasonable starting configurations. The use of coarser density fields in the first stages of the procedure allows for faster simulations to be run in terms of both computer time and the intrinsic dynamics of the systems (coarser density fields lead to faster dynamics, as will be shown later in a more quantitative and detailed manner). The procedure proposed allows for the recovery, in a few ns, of equilibrium structures going from a lower resolution of the density field to a higher one. At the first level of approximation, a very coarse density field (grid size $l = Rg$) is used to equilibrate the positions of the centers of mass of the chains and to pack them in a reasonable manner. Chain conformation and all other finer correlations are then introduced by decreasing l. The advantage of the proposed procedure based on the MD-SCF approach is that the change in model resolution is straightforward and does not involve the parametrization or rebuilding of the degrees of freedom as in the case when using coarse-grained models based on beads representing sets of atoms. This advantage allows us to solve a critical characteristic of state-of-the-art coarse-graining and reverse-mapping procedures. Indeed, these procedures are not easy to generalize and reconstruction algorithms addressing atomistic degrees of freedom depend on the specific chemistry of each polymer. In the present case, all atoms are always present, but correlations are included stepwise from *Rg* to smaller scales below the monomer scales. The procedure employed to obtain relaxed, all-atom structures is as follows:

1) Initial configurations are prepared by placing the center of mass of each chain at a random position in the simulation box. The box size is chosen according to the experimental density of the polymer bulk at the considered temperature.

2) Four subsequent relaxations using the MD-SCF approach by increasing the density field resolution (i.e., decreasing l) are performed. First, relaxation with a value for l corresponding to *Rg* (depending on the chain length) is used. The density field resolution is increased to l = 0.8 nm (∼*Rg* 10-mer) and then decreased to 0.4 (∼*Rg* 5-mer) and 0.2 nm (∼distance between two successive repeating units).

3) The structures obtained at the finest resolution, l = 0.2 nm, do not present any overlaps atoms at short distances. A very short relaxation (typically ∼100 ps for stiff polymers such as PMMA and 10 ps for softer chains such as those of PEO) using full particle resolution (full values of time steps and particle−particle potentials) is performed with standard MD simulation technique. Short relaxations of this type are sufficient to fully recover intramolecular structure parameters such as *Rg* (see next section) and the dihedral distributions (see the Supporting Information) and to obtain intermolecular correlations indistinguishable from those yielded by MD (see the next section).

In the following, the choices of the parameters used in the proposed procedures are described and validated in detail.

dx.doi.org/10.1021/ct500492h | J. Chem. Theory Comput. 2014, 10, 5651−5667

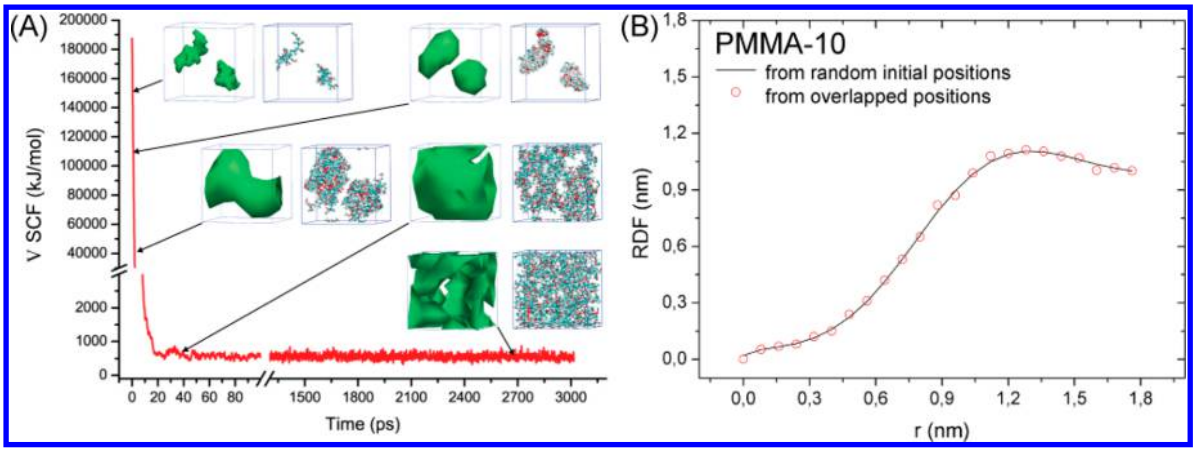

Figure 2. (A) Particle field potential vs time. (B) Equilibrium intermolecular monomer−monomer $g(r)$ calculated from simulations with as initial configuration strongly overlapped chains (red open circles) and chains randomly distributed in the simulation box (black curve). In both simulations, the density field is described using l = 0.8 nm (∼Rg of PMMA chain with N = 10).

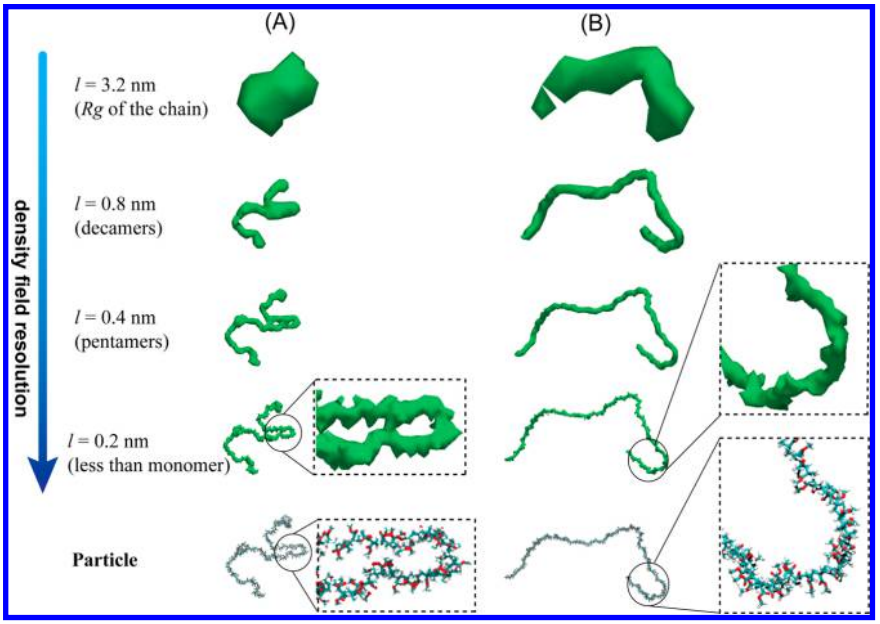

Figure 3. Density isosurfaces (describing regions in which the density is equal to $\rho_0 = N_{particles}/V_{box}$) calculated from density fields generated from a single chain of PMMA (chain length N = 180) in two different conformations (A and B) using grids of different resolution (l = 3.2 nm ∼ Rg chain, l = 0.8 nm ∼ Rg 10-mer, l = 0.4 nm ∼ 5-mer, l = 0.2 nm < monomer size).

3. RESULTS AND DISCUSSION

In addition to the intrinsic difficulties associated with the equilibration of large molecular weight polymer melts highlighted in the Introduction section, a further technical problem of traditional MD simulations is related to the setup of a suitable initial configuration (also for short chains). In particular, at typical melt densities, there are large numbers of overlaps between interacting atoms for any possible initial trial configuration. During the very early stages of simulation, a combination of energy minimizations and molecular dynamics relaxations is always needed to remove the high-energy, short-distance contacts. At this stage, in the presence of severe atom overlaps, the integration algorithm of molecular dynamics would terminate, and, typically, the procedures adopted involve a moderation of the nonbonded forces and the simultaneous use of very short time steps. For this reason, the procedures typically employed are very involved. For example, polymer chains can be placed into a simulation box at lower density, and the repulsive-excluded volume interactions are introduced smoothly by using soft-core potentials[27] or scaling on the prefactor of the repulsive part of the nonbonded potential.[75] After this stage, when a reasonable starting guess is obtained, constant-volume simulations are performed with full nonbonded potentials until typical time steps (from 1 to 2 fs) can be used, and then constant-pressure simulations are run to slowly converge to the equilibrium density. In short, the establishment of a good starting configuration is a very lengthy and tedious procedure and usually involves several trials (not all of them are successful) to obtain few initial structures.

The nature of the nonbonded interaction potential employed in the hybrid MD-SCF simulations proposed here (see eq 6) avoids this problem and does not involve any complicated procedure. In particular, even in the presence of large overlaps between particles and using large time steps, the smoothness of the forces between particles and the density field makes the MD-SCF integration very robust. To illustrate this feature, an

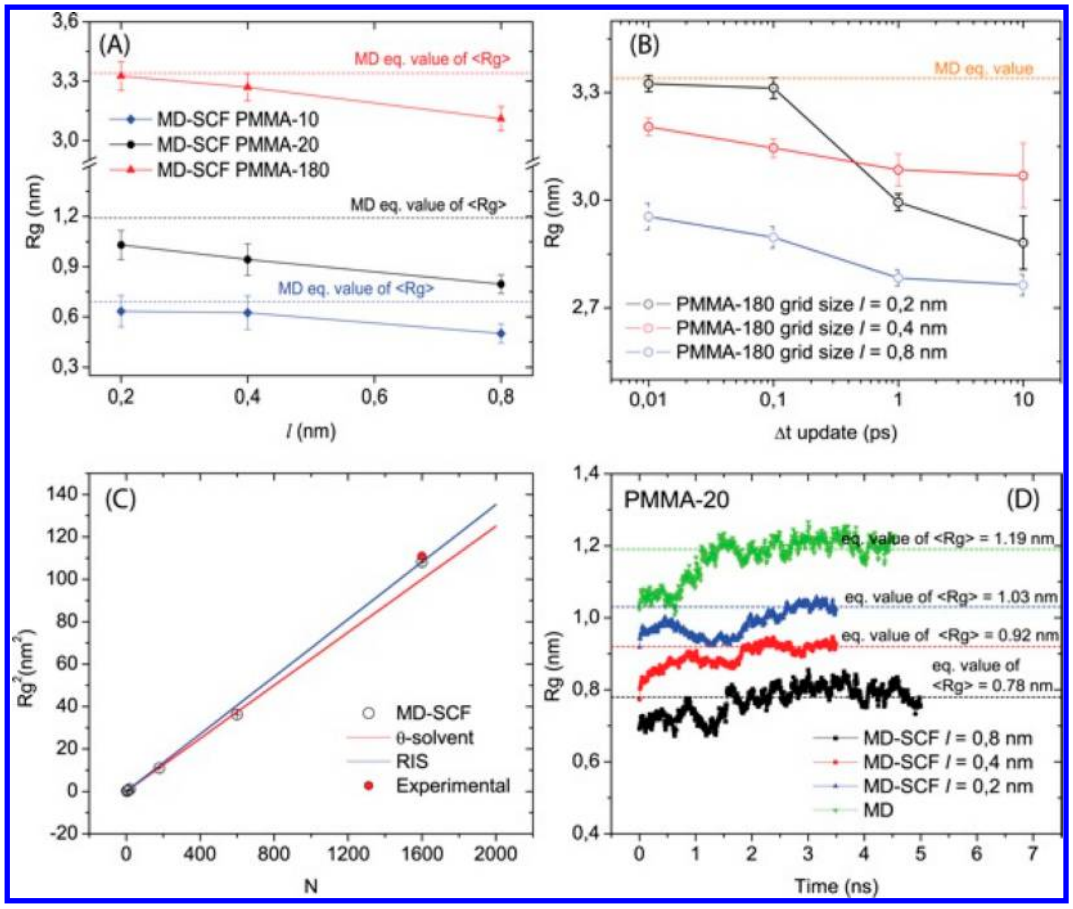

Figure 4. Equilibrium *Rg* for PMMA (A) for different chain lengths as a function of grid size *l*. (B) For different values of the density field update frequency Δt_{update}. (C) Equilibrium *Rg* for PMMA for different chain lengths calculated (l = 0.2 nm and Δt_{update} = 0.1 ps, empty circles) from experiments (red curve, analytical eq fitted from θ solvent data[76,77]) using experimental SANS data[78] (filled green circle) and the RIS calculations of Flory[79,80] (blue curve). (D) Time behavior of *Rg* for the PMMA-20 system obtained by simulations conducted at different values of grid size *l* using the equilibrium configurations derived from the closest coarse grid as the starting point.

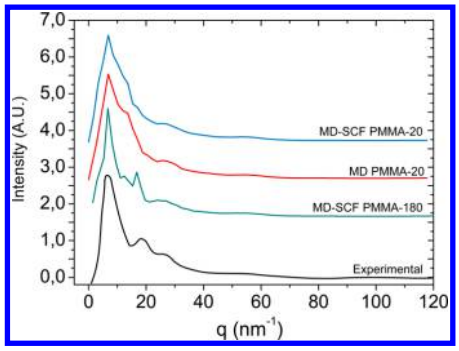

Figure 5. Experimental (X-ray)[83] and the calculated scattering intensities for polymers of two different chain lengths (PMMA-20 and PMMA-180) for systems relaxed according to the proposed procedure and using long MD simulations (PMMA-20).

MD simulation starting from an extremely overlapped configuration is reported. In a box size corresponding to the melt equilibrium density, to obtain a highly overlapped configuration, the coordinates of 30 chains are generated, replicating the coordinates of 2 chains (first snapshot in Figure 2A), i.e., in the first configuration all of the atoms of each of the two sets of 15 chains (chain length N = 10) are perfectly overlapped. In Figure 2A, the time behavior of the particle-field potential and snapshots of an MD-SCF simulation of a melt of 30 chains (10-mers) using a 1 fs time step are reported. From the figure, it is clear that polymer chains smoothly evolve toward a homogeneous distribution in the space. In Figure 2A, isosurfaces of the density field corresponding to the atomic configurations (describing regions in which the density is greater than $\rho_0 = N_{particles}/V_{box}$) are also reported. The figure clearly shows that in the first snapshot, large values of the density field are localized in very confined regions, i.e., according to eq 6, the particle field potential has a large value and particles sitting in these regions experience repulsive forces (eq 7). Thus, the equilibrium state is reached when the density field is homogeneous and the forces are related only to density fluctuations. In the simulation described in Figure 2, in approximately 1 ns, chains are homogeneously distributed in the simulation box, and after 2.5 ns, the intermolecular monomer−monomer g(r) is not distinguishable from the one obtained by equilibrating the same system starting from a configuration with randomly distributed polymer chains. In the latter case, equilibration is much faster, and the equilibrium monomer−monomer g(r) is obtained in ∼40 ps.

As reported in section 3, the density field is calculated on the fly (with a given update frequency) from particle positions and is defined on a tridimensional grid. The grid step l is an important parameter defining the resolution of the density field. The larger the value of l is, the greater the number of particles that are included in a single cell and the coarser the description

dx.doi.org/10.1021/ct500492h | J. Chem. Theory Comput. 2014, 10, 5651−5667

Table 2. Simulation Times Required To Recover Different Structural Correlations

		MD-SCF $l = Rg \rightarrow 0.8$ nm[a] (ns)[a]			MD-SCF $l = 0.8 \rightarrow 0.4$ nm[a] (ns)[a]			MD-SCF $l = 0.4 \rightarrow 0.2$ nm[a] (ns)[a]			
system	τ_{Rg} (ns)	*M*	*P*	*D*	*M*	*P*	*D*	*M*	*P*	*D*	MD-SCF $l = 0.2 \rightarrow$ MD[b] (ps)[b]
PMMA-5	0.08							2.0	2.3		11.0
PMMA-10	0.87	3.7	3.8		1.9	2.2		2.5	2.9		11.0
PMMA-20	1.55	3.4	4.1	4.0	1.7	2.4	2.6	2.1	2.9	2.9	11.0
PMMA-180	7.92	3.9	4.2	4.7	1.9	2.4	2.3	2.4	2.7	2.9	11.0
PMMA-400	41.3	4.1	4.1	4.6	2.3	2.7	2.8	2.9	3.1	2.8	11.0
PMMA-600	88.5	4.4	4.2	4.4	2.2	2.4	2.6	2.4	2.9	2.9	11.0

[a]Time to fully recover $g(r)$, starting from equilibrated configurations with coarser density field description at M = monomer, *P* = pentamer, *D* = decamer level. [b]Time required to fully recover atom−atom $g(r)$ calculated by classical MD simulations from configurations equilibrated with MD-SCF using the highest density field resolution (l = 0.2 nm). Radial distribution functions showing how the proposed procedure is able to recover structural correlations are reported for the PMMA-180 system as an example in the Supporting Information (Figure S2). In the case of PMMA further 70 ps are needed to recover dihedral distributions (see Figure S5 in the Supporting Information).

Table 3. Simulation times (ns) and Corresponding Computational Cost (in Terms of CPU Hours) for Relaxation of a System of 100 PMMA Chains (N = 180, 270200 Atoms)[a]

	simulation length	CPU hours
1st stage $l = Rg$	20 ns	12 h
2nd stage l = 0.8 nm	5 ns	3 h
3rd stage l = 0.4 nm	5 ns	3 h
4th stage l = 0.2 nm	5 ns	3 h
full MD short relaxation	100 ps	∼5 min
total	∼35.1 ns	∼21 h

[a]The computational cost corresponds to that of a simulation using a parallel version of OCCAM[62] employing 96 processors Intel Xeon E5620.

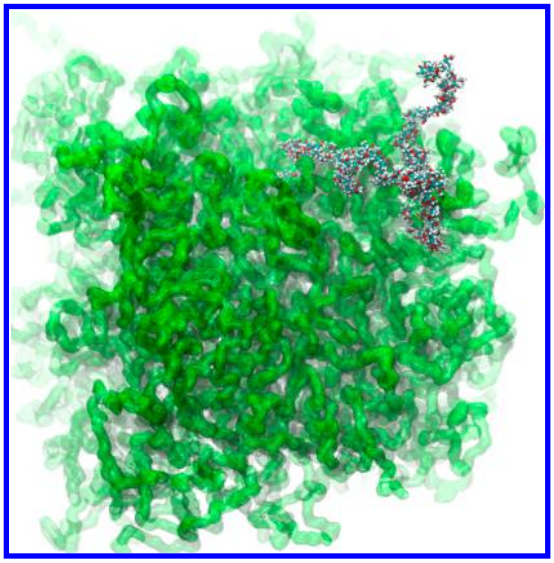

Figure 6. Snapshot of the PMMA-180 system composed of 100 chains of PMMA with N = 180. Only a single full-atom chain is depicted explicitly with carbon (blue), oxygen (red), and hydrogen (white) atoms in the density field (green). The density field is visualized using the density isosurfaces of the chain backbones.

of the density field with respect to the underlying particle model becomes. To better explain this aspect, in Figure 3, the density field, shown as an isosurface (describing regions in which the density is equal to than $\rho_0 = N_{particles}/V_{box}$) calculated from two different configurations (different conformers) of an all-atom model of a single chain of PMMA (chain length N = 180) at three different resolutions, is depicted. The figure clearly shows that with a resolution of 0.8 nm (close to the radius of gyration of 10 repeating units) the main shape of the chain backbone is described and the isosurface is quite smooth (see Figures 3A and 3B), whereas when using a finer resolution, it is possible to describe the presence and the bulkiness of substituents as well. As shown in Figure 3, in going from l = 0.4 (5-mer *Rg*) to l = 0.2 nm (∼ distance between two successive repeating units), asperities due to the bulkiness of the backbone substituents are also described by the shape of the density field. In particular, the insets of Figure 3, which compare the details of the isosurface corresponding to the density field calculated for l = 0.2 nm and the atomic structure, make this feature apparent.

Thus, the proposed procedure involves subsequent system relaxations via MD-SCF simulations using different grid resolutions.

Although MD-SCF simulations are conducted at the equilibrium density, the structures obtained at the finest resolutions (typically l = 0.4 and 0.2 nm) do not present any atom superposition at short distances. Therefore, a short relaxation using MD by full time steps and pair potentials can be readily performed, yielding structures that are completely indistinguishable from those obtained using long MD simulations.

Gyration radii obtained from simulations using l = 0.2 nm for PMMA melts at T = 500 K with different chain lengths, as a function of molecular weight up to 1600 repeating units, are compared with experimental data obtained from theta solutions of PMMA,[76,77] SANS data for polymer melts,[78] and RIS calculations reported by Flory[79,80] in Figure 4C. The figure clearly demonstrates good agreement between the MD-SCF simulations and experimental measurements over the entire range of molecular weights considered. For example, for N = 1600, the calculated *Rg* is 10.4 nm, and the experimental values measured using the SAXS technique in the bulk by Krishnamoorti et al.[78] are 6 and 10.1 nm under the θ-conditions reported by O'Really.[77] It is worth noting that, as will be shown in the following, we can also achieve an efficient relaxation of atomistic models for molecular weights comparable with those employed for commercial use.[81]

dx.doi.org/10.1021/ct500492h | J. Chem. Theory Comput. 2014, 10, 5651−5667

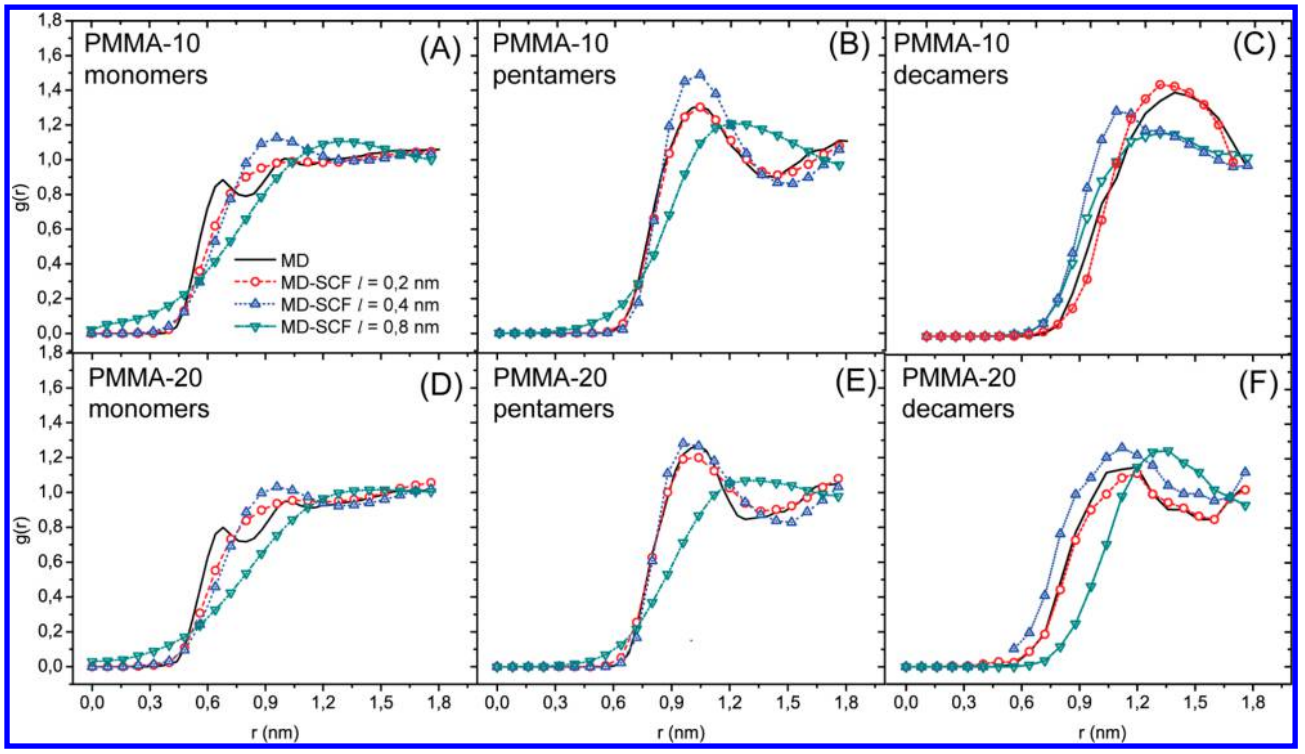

Figure 7. Comparison of intermolecular radial distribution functions between MD and MD-SCF simulations, at different grid sizes, calculated with respect to the centers of mass of monomers, pentamers, and decamers, respectively, for PMMA-10 (A−C) and PMMA-20 (D−F). The results obtained for the PMMA-5 system are reported in the Supporting Information (Figure S3).

As presented for the single-chain properties in PMMA melts, in Figure 4A, the behavior of *Rg* as a function of grid size for other systems (PMMA-10, -20, and -180) is reported. For all cases, a finer resolution of the grid corresponds to an increase in *Rg* and values closer to those measured in experiments. This behavior demonstrates how a finer grid resolution corresponds to a better description of excluded volume interactions (bulkiness of substituents, interactions between atoms along the same chain such as 1−4, 1−5 and between different chains). Similar behavior is observed for the update frequency (Figure 4B); specifically, for $\Delta t_{update} < 1$ ps, where the value of *Rg* for PMMA-180 converges to the MD value. Using large grids corresponds to a coarser description of molecular shapes, softer potentials and forces. Implementing a large grid means collecting a large number of particles in a single cell when the coarse-grained density field $\phi(\mathbf{r})$ is built. A coarser description of short-range correlations along the chains leads to a systematic underestimation of *Rg*, and the use of finer grids leads to a systematic improvement of *Rg*. To clarify this behavior and to validate the proposed procedure, in Figure 4D, the time behavior of *Rg* for the PMMA-20 system is reported. The aim of this figure is to show how long the relaxation of *Rg* is in going from coarser density resolutions to finer ones and from the finest density resolution (l = 0.2) nm to MD. This plot clearly demonstrates that *Rg* increases by 10% in going from l = 0.8 to 0.4 nm. The same trend occurs in going from l = 0.4 to 0.2 nm and, finally, in going from l = 0.2 to MD; the increase is approximately 20%. Although a substantial deviation is also observed for the smallest grid sizes, in all cases, due to the softness of the potential and the fast relaxation of low molecular weight models, the simulation length that is able to recover the equilibrium value of *Rg* in going from one scale to another is between 2 and 3 ns and always below 5 ns. Such an underestimation of *Rg* would be a critical result if large molecular weight melts would follow the same behavior. It is interesting that the agreement for all grids is high in the case of high molecular weight. For example, as reported in Figure 4A, for the PMMA-180 system, going from $l = Rg$ to 0.8 nm yields an 8% increase in *Rg*, going from l = 0.8 to 0.4 nm yields a 3% increase, and the deviation from l = 0.2 to full MD is only 1%. In the Supporting Information (Figure S6), plots of the time behavior of *Rg* analogous to the ones reported in Figure 4D is shown for the PMMA-180 system. Plots of Figure S6 show that these small deviations from the MD structures for high molecular weights allow for the recovery of the correct structures in short times (>1 ns). This behavior is not surprising and can be rationalized considering the high accuracy of mean-field approximations at large molecular weights. In particular, in addition to the grid size and update frequency, the invariant degree of polymerization $\tilde{N}$ is a relevant quantity for the behavior of dense polymer melts. In a dense melt, for which $Rg = bN^{1/2}$ (where b is the Kuhn length and N is the number of repeating units), this quantity is $\tilde{N} = (\rho_0 b^3)^2 N$ (where ρ_o is the average number density of repeating units). The value of $\tilde{N}$ allows for the quantification of the number of neighboring molecules with which a reference chain interacts. In the limit $\tilde{N} \rightarrow \infty$, the fluctuations of the collective density are strongly suppressed such that the approximations used in self-consistent field theory become accurate.[51,82] Comparison with experimental data indicates that the approximations are safe for values of $\tilde{N} > 10^4$.[51,82] In the present case, values of $\tilde{N} > 10^4$ would correspond to $N > 21$ for PMMA (b = 1.53 nm). This increase in accuracy with molecular weight has important practical advantages. Indeed, for low molecular weights, for which larger deviations are expected, relaxations are faster, and the last stage of the procedure, involving full MD simulations, is

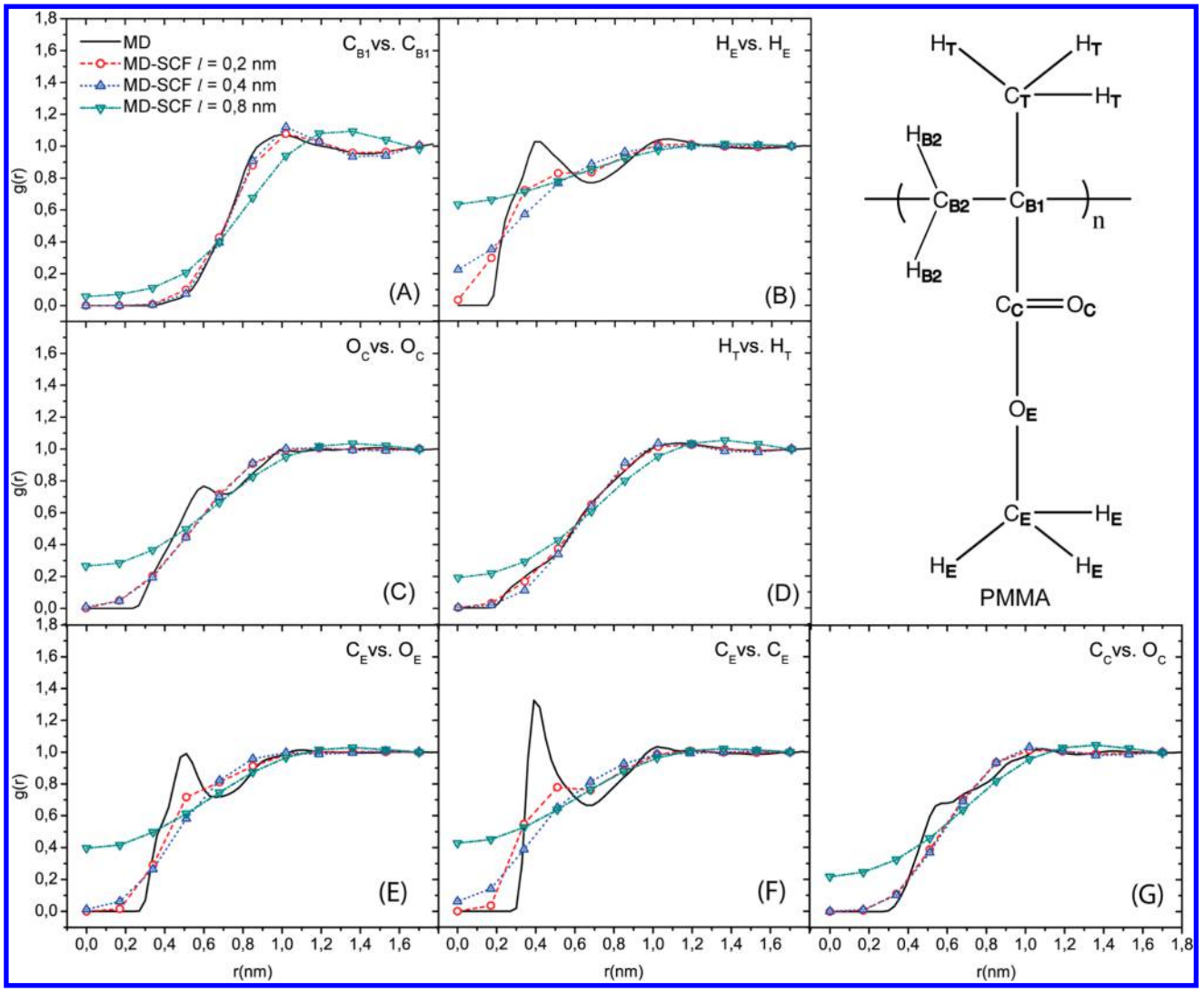

Figure 8. Comparison of intermolecular radial distribution functions between MD and MD-SCF for different atom pairs (different atom types are defined in the top right corner of the figure).

feasible. On the other hand, for large molecular weights, for which relaxations are slower, the structures obtained at the MD-SCF level are very similar to the equilibrium values of MD. Similar features have been observed for radial distribution functions (see discussion later).

Chain packing can be validated by comparing calculated and experimental X-ray scattering data. In Figure 5, the experimental and calculated scattering intensities for oligomers and for melts with longer chains are reported. A useful comparison to make is that between scattering data obtained from oligomer melts using "brute force" MD relaxation. The short chain length can ensure that a full relaxation can be obtained using the standard MD approach. In fact, for this system, for a simulation period of 20 ns, every chain is able to move over an average of approximately 7 times its radius of gyration, and the corresponding end-to-end relaxation time (3 ns estimated using autocorrelation functions) is shorter than the simulation length. Figure 5 shows that the scattering intensities obtained from full MD relaxation and from the proposed procedure are practically coincident with those obtained by experiment. As will be discussed in the section, for longer chain lengths, the relaxation time grows rapidly to large values that practically make "brute force" MD chain relaxation impossible. The advantage of the proposed procedure is the feasibility of system relaxation due to the weak dependence of relaxation time on chain length, which is associated with the very smooth nature of the particle field interactions. In Figure 5, the X-ray scattering calculated from simulations of the PMMA-180 system relaxed according to the proposed procedure is reported. It is interesting to note that in this case a better reproduction of the experimental scattering intensity is obtained. Likely due to the higher molecular weight considered, the region at low q is better reproduced. In particular, in agreement with the experimental scattering intensity, the second peak at approximately 19.3 nm^{-1} is more apparent, whereas in both "brute force" relaxed and particle-field oligomeric systems, only a shoulder close to the most intense peak at 9.81 nm^{-1} is observed.

In Table 2, information related to the proposed procedure for PMMA systems with different chain lengths is summarized. In particular, τ_{Rg} shows the simulation time required to move every chain in the system by a distance at least equal to one *Rg*, as can be calculated from the mean square displacement (MSD) of the chain center of mass in simulations using coarse density resolution ($l = Rg$, corresponding to the chain length). The simulation times required to recover decamer−decamer

dx.doi.org/10.1021/ct500492h | J. Chem. Theory Comput. 2014, 10, 5651−5667

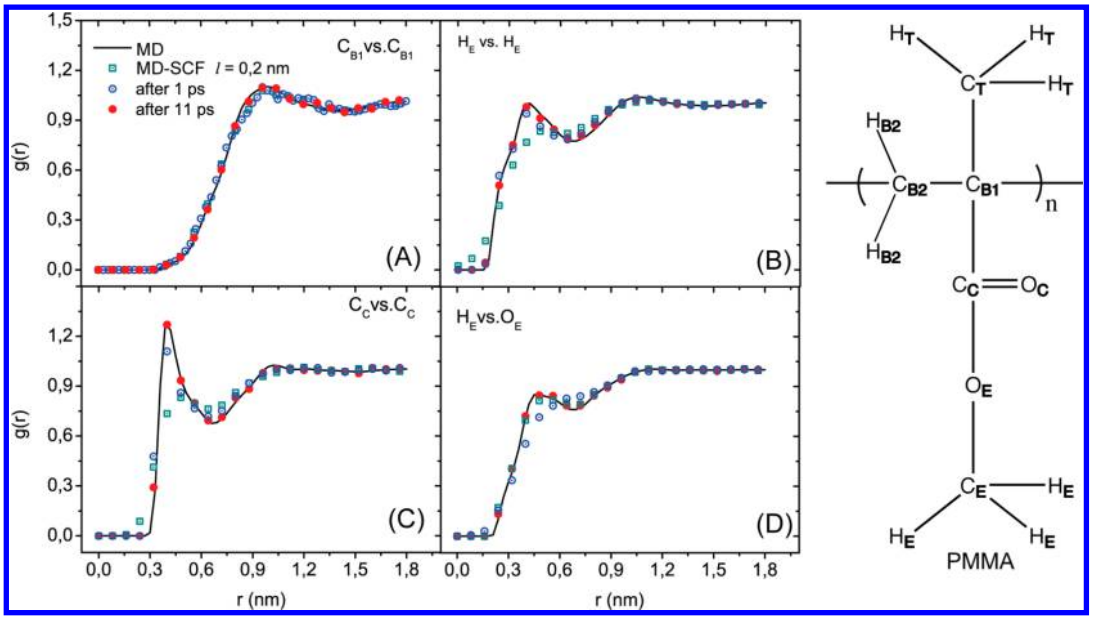

Figure 9. Comparison of intermolecular radial distribution functions, for different atom pairs, between MD (black line), MD-SCF (green squares), and MD-SCF configurations after reintroduction of short-range interactions (blue circle = 1 ps, and filled red circle = 11 ps).

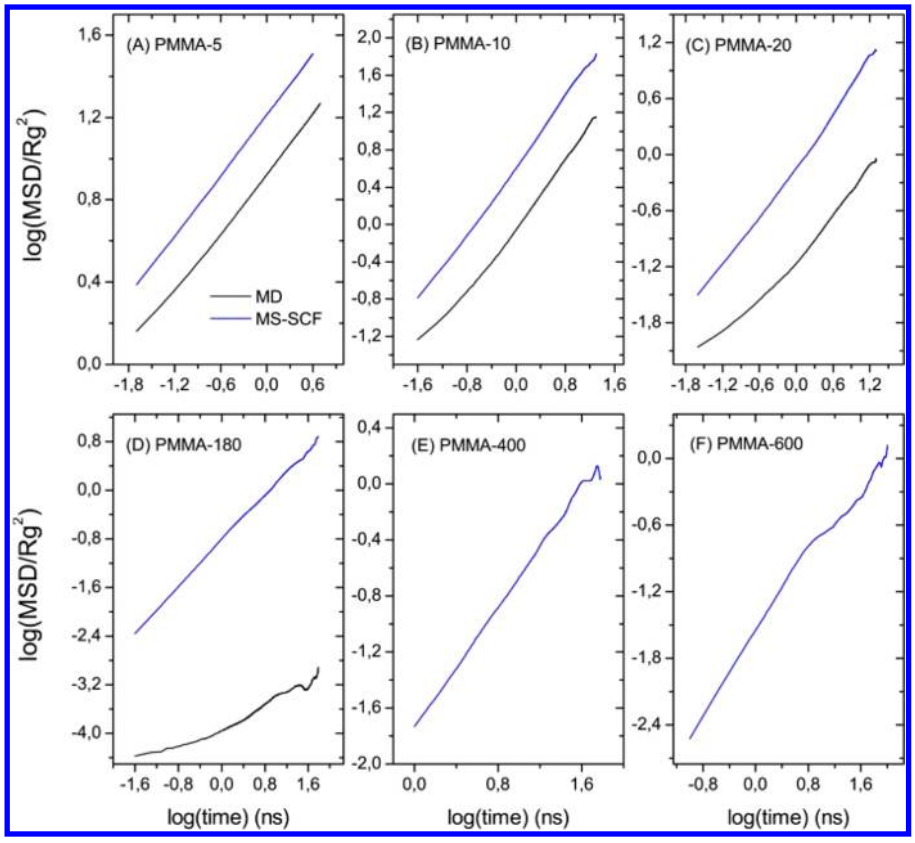

Figure 10. Mean square displacement of the center of mass of PMMA chains as a function of time. MD-SCF simulations were conducted using $l = Rg$ and $\Delta t_{update} = 0.1$ ps.

(indicated as *D* in Table 2), pentamer−pentamer (indicated as *P* in Table 2), monomer−monomer (indicated as *M* in Table 2), and atom−atom (last column of Table 2) radial distribution functions from the closest coarser level of density resolution are also reported. As reported in Table 2, the largest differences are in the simulation lengths of the first stage performed using the coarsest density description ranging from hundreds of ps (for low molecular weights) to ∼90 ns (for the highest molecular weight). For more local relaxations, related to length scales ranging from those of decamers to those of monomers, there is no apparent dependence on molecular weight, and the simulation time correlations are consistently on the order of a few ns. In particular, as reported in Table 2, the simulation times required to fully recover structural correlations at the

dx.doi.org/10.1021/ct500492h | J. Chem. Theory Comput. 2014, 10, 5651−5667

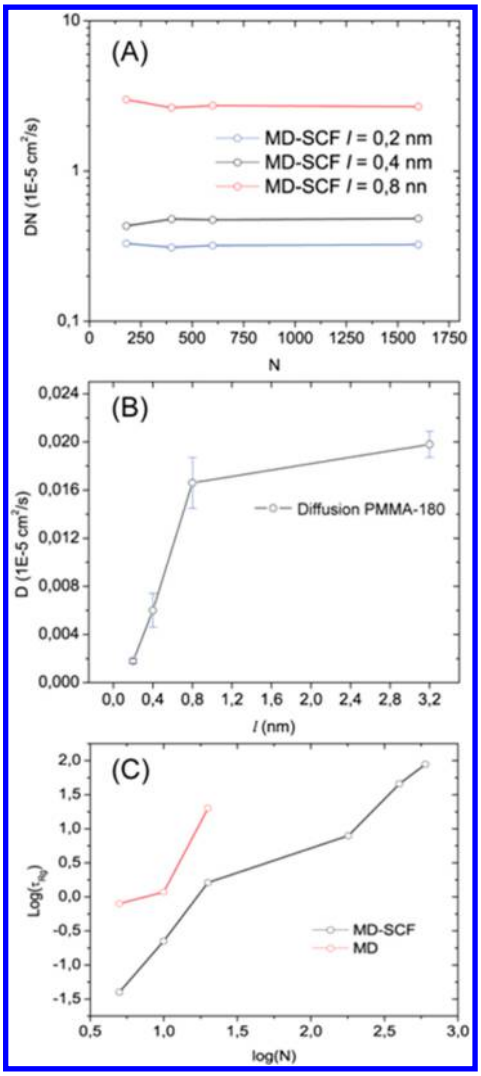

Figure 11. (A) Diffusion coefficient of the centers of mass of chains as a function of number of monomers N per chain. (B) Diffusion coefficient of the centers of the mass of PMMA-180 chains as a function of grid size l. (C) τ_{Rg} as a function of N for MD-SCF and MD simulations.

pentamer and monomer levels for MD-SCF simulations with l = 0.8 nm starting from $l = Rg$ for times ranging from 3 to 4 ns (third column of Table 2) and for MD-SCF going from l = 0.8 to 0.4 and from 0.4 to 0.2 nm for times ranging from 1 to 3 ns (fourth and fifth columns of Table 2). Finally, pair correlations between atoms are fully recovered with very short MD relaxations (11 ps, last column of Table 2). Pair correlations are considered to be recovered if the deviation between the equilibrium $g(r)$ and the calculated values is less than 3%. A quantitative definition of the deviation (eq S15) and a tabulation of such values (Table S9) can be found in the Supporting Information.

It is worth noting that after this procedure, the structures relaxed at the experimental density of PMMA melts in the *NVT* ensemble do not show any change in average density in *NPT* simulations. As an example, the density behavior observed in a *NPT* simulation of the PMMA-20 system at 500 K and 1 atm is reported in the Supporting Information (Figure S4).

According to these results, a sample application of the proposed procedure, together with the simulation times and real time required for the computations, is described in Table 3 for a system composed of 100 chains of PMMA (chain length N = 180, 270200 atoms). Figure 6 shows a model of such a system in which all polymer chains are represented by the density isosurfaces, and only a single chain is reported in all-atoms configuration.

It is interesting to analyze, in greater depth, the behavior of structural correlations by observing them at different scales ranging from the decamer to the monomer and finally to the atomic scale and how these levels of detail are captured by the MD-SCF simulations for different values of l. For PMMA, we can consider an Rg value corresponding to N = 10 (~0.8 nm) to be representative of the decamer length scale, an Rg value of approximately 0.4 nm to be representative of the pentamer length scale, and the average distance between two consecutive repeating units (~0.2 nm) to be representative of the monomer length scale.

In Figure 7, the intermolecular $g(r)$ values between effective particles obtained by grouping atomic coordinates along the chains as decamers, pentamers, and monomers are reported for PMMA with N = 10 (Figures 7A–C) and N = 20 (Figures 7D–F). It is interesting to observe that for $l \leq 0.4$ nm, the MD-SCF simulations yield correlations similar to those of the MD simulations based on pair potentials. In particular, for a grid size l = 0.8 nm, a partial superposition of monomers is obtained for both systems, N = 10 and 20 (the $g(r)$ at r = 0 has a small but finite value in Figures 7A and 7B). For smaller grid sizes, the typical correlation hole of the $g(r)$ value of polymer melts is well reproduced at the monomer level as well.

Figure 8 compares the intermolecular atomic pair correlation functions obtained by MD and MD-SCF simulations. It is interesting to observe that the correlations between atoms along the backbone are already very well reproduced using a grid resolution l = 0.4 nm (see Figure 8A). Similar behavior can be observed for atoms close to the backbone (see Figures 8C, 8D, and 8G). Deviations from MD simulations are observed for atoms far from the backbone and/or belonging to polar groups. This behavior can be explained by considering that the correlation between atoms in the backbone is not direct but is mediated through interactions between substituents, whereas the interactions between lateral groups depend more on interactions between particle pairs. In other words, the backbone correlations are "less pairwise" than the correlations between lateral groups, and they can be properly described using the density field. However, in the case of the substituents, the short-range behavior, which in the MD simulations is dictated by excluded volume interactions, is reasonably reproduced for the highest grid resolution (l = 0.2 nm). The peaks in $g(r)$ of atoms belonging to polar groups, due to our choice to disregard terms depending on the χ_{KK}' parameters, cannot be reproduced. As will be demonstrated in the following, these correlations have a very local nature and can be recovered using very short relaxations. In fact, Figure 9 shows pair correlation functions obtained from simulations performed in the last stage of the proposed procedure. These simulations use the configurations equilibrated using the MD-SCF approach with l = 0.2 nm for MD relaxations lasting a few ps. The figures clearly show that 11 ps is enough to recover the full correlation for pairs with intense peaks in $g(r)$.

Dynamic Properties. The largest time scale to consider in the equilibration of a polymer melt is typically related to the diffusion process of the center of mass of an entire chain. In particular, a procedure can be considered effective if during the

dx.doi.org/10.1021/ct500492h | J. Chem. Theory Comput. 2014, 10, 5651–5667

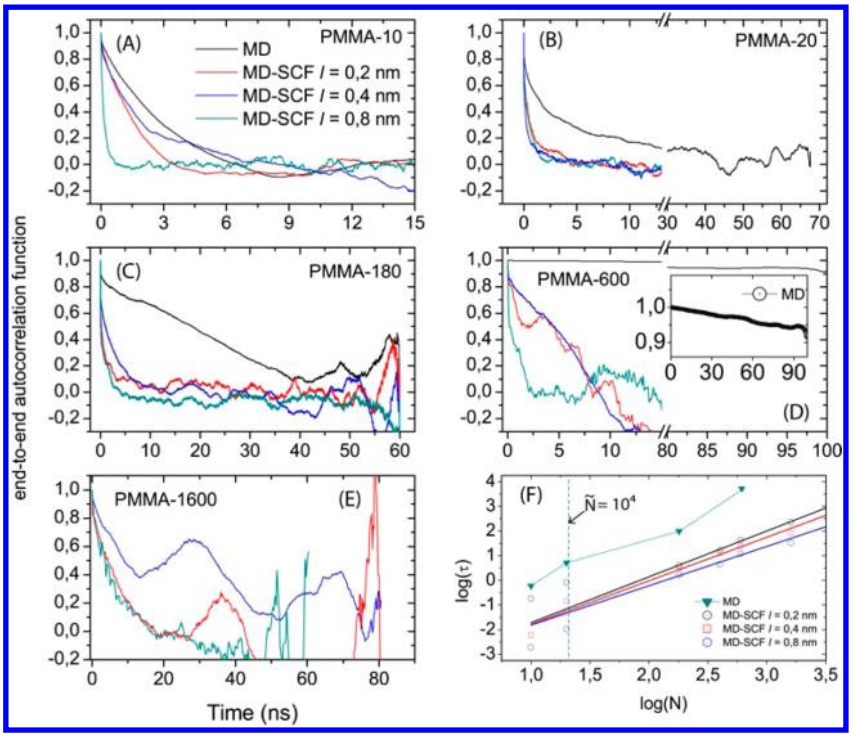

Figure 12. End-to-end autocorrelation functions for systems with increasing number of monomers N per chain from 10 to 1600 (A-E). (F) End-to-end relaxation time τ as a function of N for MD and MD-SCF simulations.

Table 4. Fitting Parameters for Chain Diffusion (τ_0, Second Column) and End-to-End Relaxation (τ_0 and Exponent, Third Column)

grid size l (nm)	$\tau_0{}^a$ (ps)	$\tau_0{}^b$ (ps)	exponent^b
0.2	8.4	0.3	1.9
0.4	7.2	0.3	1.8
0.8	5.0	0.4	1.6

[a]Fitted from diffusion data of Figure 8A. [b]Fitted from end-to-end relaxation times of Figure 9F.

equilibration of each chain it is possible to move its center of mass by at least the length of its size (i.e., Rg). Based on this metric, in Figure 10, a nondimensional quantity obtained from the logarithm of the mean square displacement of the chain center of mass (in units of Rg^2) as a function of simulation time is reported for several systems with different PMMA chain lengths (as log−log plot). In the figure, times corresponding to values greater than or equal to zero on the y axis indicate simulation lengths sufficient for equilibration.

As expected, in going from short to longer chain lengths, the time required for equilibration increases. In the case of the MD simulation, a reliable equilibration is possible only for chain lengths smaller than 100 units. Beyond this length, entanglements between chains slow down the diffusion process. The plots shown in Figure 10 corresponding to the MD results (black lines) indicate that a few nanoseconds are enough to equilibrate short oligomers (PMMA-10 and PMMA-20). For the PMMA-20 system, 20 ns is already sufficient, and for the longer PMMA-180 system, in 40 ns, displacement does not take place.

It is interesting to examine the behavior of diffusion coefficients as a function of the chain length for the MD-SCF models. In particular, in Figure 11A, the diffusion coefficients of the chain center of mass ($D \times N$) is plotted as a function of the chain length N for three different values of the density resolution. The behaviors exhibited in the three cases are very similar, and the curves are simply shifted according to the grid size. In particular, diffusion is slow for small density grid sizes. This behavior is reasonable because the potential becomes less smooth when finer details of the polymer chains are described. This effect has already been reported for MD-SCF coarse-grained models of lipids.[55,56] An important feature of these results is the absence of any entanglement effect. In fact, for large values of N as well, the diffusion follows a Rouse behavior (D scales as N^{-1}). In Figure 11C, the behavior of the chain diffusion time τ_{Rg} as a function of chain length is reported. As previously described, for each system, as a function of chain size (Rg), the first relaxation stages involve MD-SCF simulations for $l = Rg$. Thus, although for large values of N the diffusion is slower and larger displacements are needed to complete the first stage of equilibration, two main compensating effects are observed in the MD-SCF simulations. Both the intrinsic time scale of the models and the simulation cost per time step are small for systems with long chain lengths. In particular, Figure 11B reports the behavior of the diffusion coefficient as a function of the grid size l. The diffusion of $l = Rg$ is approximately 10 times faster than that in the last stage of the chain relaxation performed at $l = 0.2$ nm and in all cases much faster than that in the MD simulations. These advantages, due to the absence of entanglement effects, are more pronounced for long chain lengths. With respect to the simulation costs, as previously tested for several systems, the use of large grid sizes, especially for large systems, leads to more efficient parallel performances of the code in terms of both communication and computational time.[62]

To understand the efficiency of the relaxation process, another important time scale is the one related to the relaxation of the end-to-end distance. In Figures 12A−E, autocorrelation functions of the end-to-end vector are reported for systems

dx.doi.org/10.1021/ct500492h | J. Chem. Theory Comput. 2014, 10, 5651−5667

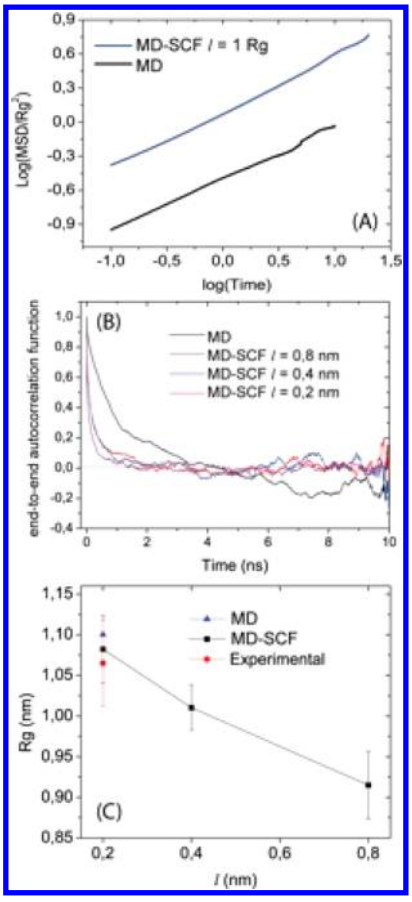

Figure 13. (A) Average center of mass mean square displacement (MSD) of PEO chain as a function of time. The nondimensional quantity on the vertical axis is the mean square displacement of the center of mass in units of Rg^2. MD-SCF simulations were conducted using $l = Rg$ and Δt_{update} = 0.1 ps. (B) End-to-end autocorrelation function of PEO for MD and MD-SCF simulations. (C) Behavior of radius of gyration of PEO as a function of the grid size l. The experimental SANS value[68] (filled red circle) and the value calculated by MD simulations (filled blue triangle) are also reported on the plot.

with different chain lengths. From the figure, it is clear that MD-SCF simulations are characterized by a fast decrease in the correlation functions and provide faster chain relaxations with respect to MD simulations. As the chain length increases, the difference between chain relaxation processes in MD and MD-SCF simulations becomes greater. Furthermore, the effect of the grid size l on the relaxation of the end-to-end vector is similar to that obtained for diffusion (a large value of l corresponds to a fast process) and is also, in this case, related to the smoothness of the potentials for large values of l. In Figure 12F, the relaxation times of the end-to-end vector calculated by an integration of a stretched exponential fitted from the autocorrelation functions of Figure 12A−E, as described in eq 9, are shown.

$$\tau = \int_0^\infty \exp\left[-\left(\frac{t}{\alpha}\right)^\beta\right] dt = \frac{\alpha}{\beta}\Gamma\left(\frac{1}{\beta}\right) \tag{9}$$

It is interesting to note that, independently of the grid size, for MD-SCF simulations the relaxation times follow a power low of the type $\tau \approx \tau_0 N^2$. This feature is consistent with the absence of entanglement effects obtained from diffusion coefficients (Rouse behavior in Figure 11A). A quantitative evaluation of both the exponent and prefactors was performed for both the diffusion coefficients and end-to-end relaxation times.

For the diffusion process, Figure 11A shows that the curve of DN vs N is practically constant. From the value of DN obtained according to the Rouse model, we can estimate the friction coefficient for chain diffusion ζ

$$D_R N = kT/\zeta \tag{10}$$

and using the value of the Kuhn length b of PMMA we can obtain

$$\tau_0 \approx \zeta b^2/kT \tag{11}$$

From end-to-end correlation times, both τ_0 and the exponent can be fitted by a linear interpolation of the log−log plots reported in Figure 12F. It is interesting to note that the data corresponding to molecular weights of $N < 10^4$ (i.e., $N < 21$, see discussion about the accuracy of mean-field approximations reported above) do not align with the data corresponding to high molecular weights. In addition, in this case, for molecular weights lower than 21, the effect of density fluctuations is not properly described by mean-field approximations. For this reason, these points have been excluded from the fitting. Another interesting effect is that the smaller l is, the closer the exponent fitted from end-to-end correlation times to the theoretical predictions for the Rouse behavior becomes. In Table 4, we report the τ_0 values obtained using different grids for both chain diffusion and end-to-end relaxation.

These results indicate that the relaxation process obtained using the MD-SCF approach for high molecular weights has a weaker dependence on chain length than that obtained using MD simulations (where $\tau \approx \tau_0 N^3$), and computational costs of the proposed procedure are mainly related to the system size rather than the chain length.

PEO Melts. In this section, we present the results obtained for PEO melts by applying the same procedure described in detail for PMMA. It should be stressed that the procedure is parameter-free. Without considering the effect of the $\chi_{KK'}$ parameters, the only parameter is the compressibility. This parameter depends mainly on the scale of the models and their density fluctuations and is safely transferable. In fact, the value used in the present study is the same as the values used in previous studies for coarse-grained models of lipids[55−58] and for mixtures of Pluronics and water.[44]

The behaviors obtained for PEO are similar to those reported in the previous section (see Figures 13A−C). Moreover, in this case, short relaxations with MD simulations are sufficient to fully recover the fine structure of $g(r)$ (see Supporting Information section S3), and the total intermolecular $g(r)$ obtained using the proposed procedure is coincident with the one reported by Smith[66] and Maranas[67] for PEO melts (see Supporting Information section S3).

CONCLUSIONS

A procedure based on MD-SCF simulations able to generate well-relaxed all-atom structures of polymer melts has been proposed. The application of this procedure to two different all-atom polymer models, PMMA and PEO, was reported and validated. In particular, all-atom structures with a structural correlation indistinguishable from the correlations obtained by long MD relaxations can be achieved.

dx.doi.org/10.1021/ct500492h | J. Chem. Theory Comput. 2014, 10, 5651−5667

Due to the efficiency of parallel applications, the computational cost of the proposed approach is very low. This aspect, together with the fast dynamics, due to the softness of MD-SCF models, in practice leads to computational costs that are mainly to the system size rather than to the chain length.

It is important to stress that, according to the proposed procedure, no parametrization is needed to generate relaxed structures of different polymers (no use of χ parameters for homopolymer melts).

Moreover, due to the nature of the MD-SCF scheme, the field is a byproduct of particle positions (i.e., all the particles are always present in the model), unlike in current coarse-graining strategies based on particle reductions, and there is no need for special algorithms or back-mapping schemes to change the resolution of the models. This feature makes the proposed procedure general and its extension to other polymer architectures straightforward.

Finally, a similar procedure can be easily extended to the generation of all-atom structures of systems more complex than homopolymer melts. In particular, similarly to several hybrid MD-SCF models already reported in the literature,[44,60,61] for block copolymers and for polymer nanocomposites[49,84] all-atom structures can be obtained using few χ parameters by modeling the repulsive interactions between incompatible phases.

■ ASSOCIATED CONTENT

Supporting Information

Sections S1−S3 containing Tables S1−S9 and Figures S1−S10. This material is available free of charge via the Internet at http://pubs.acs.org.

■ AUTHOR INFORMATION

Corresponding Author

*E-mail: gmilano@unisa.it.

Notes

The authors declare no competing financial interest.

■ ACKNOWLEDGMENTS

G.M. thanks MIUR (TECOP - Tecnologie di produzione di composti a matrice polimericai, project PON02_00029_3206010) for the financial support and the HPC team of ENEA for using the ENEA-GRID and the HPC facilities CRESCO (www.cresco.enea.it) in Portici, Italy.

■ REFERENCES

(1) Flory, P. J. *Principles of Polymer Chemistry*, 1st ed. ed.; Cornell University Press: Ithaca, NY, United States, 1953.

(2) Flory, P. J. *Statistical mechanics of chain molecules*; Interscience: New York, 1969.

(3) de Gennes, P. G. *Scaling Concepts in Polymer Physics*; Cornell University Press: Ithaca, NY, 1979.

(4) Mansfield, K. F.; Theodorou, D. N. Atomistic Simulation of a Glassy Polymer/Graphite Interface. *Macromolecules* **1991**, *24* (15), 4295−4309.

(5) Mansfield, K. F.; Theodorou, D. N. Atomistic Simulation of a Glassy Polymer Surface. *Macromolecules* **1990**, *23* (20), 4430−4445.

(6) Smith, G. D.; Paul, W.; Monkenbusch, M.; Richter, D. A Comparison of Neutron Scattering Studies and Computer Simulations of Polymer Melts. *Chem. Phys.* **2000**, *261* (1−2), 61−74.

(7) Tsolou, G.; Mavrantzas, V. G.; Theodorou, D. N. Detailed Atomistic Molecular Dynamics Simulation of Cis-1,4-poly(butadiene). *Macromolecules* **2005**, *38* (4), 1478−1492.

(8) Eslami, H.; Müller-Plathe, F. Structure and Mobility of poly(ethylene terephthalate): A Molecular Dynamics Simulation Study. *Macromolecules* **2009**, *42* (21), 8241−8250.

(9) Eslami, H.; Kesik, M.; Karimi-Varzaneh, H. A.; Müller-Plathe, F. Sorption and Diffusion of Carbon Dioxide and Nitrogen in Poly(methyl methacrylate). *J. Chem. Phys.* **2013**, *139* (12), 124902.

(10) Auhl, R.; Everaers, R.; Grest, G. S.; Kremer, K.; Plimpton, S. J. Equilibration of Long Chain Polymer Melts in Computer Simulations. *J. Chem. Phys.* **2003**, *119* (24), 12718−12728.

(11) Fritz, D.; Herbers, C. R.; Kremer, K.; van der Vegt, N. F. A. Hierarchical Modeling of Polymer Permeation. *Soft Matter* **2009**, *5* (22), 4556−4563.

(12) Vettorel, T.; Grosberg, A. Y.; Kremer, K. Statistics of Polymer Rings in the Melt: A Numerical Simulation Study. *Phys. Biol.* **2009**, *6* (2), 025013.

(13) Milchev, A.; Binder, K. Adsorption of Oligomers and Polymers into a Polymer Brush Formed from Grafted Ring Polymers. *Macromolecules* **2013**, *46* (21), 8724−8731.

(14) Rutledge, G. C.; Suter, U. W. Calculation of Mechanical Properties of Poly(p-phenylene terephthalamide) by Atomistic Modelling. *Polymer* **1991**, *32* (12), 2179−2189.

(15) Barrat, J.-L.; Baschnagel, J.; Lyulin, A. Molecular Dynamics Simulations of Glassy Polymers. *Soft Matter* **2010**, *6* (15), 3430−3446.

(16) Anogiannakis, S. D.; Tzoumanekas, C.; Theodorou, D. N. Microscopic Description of Entanglements in Polyethylene Networks and Melts: Strong, Weak, Pairwise, and Collective Attributes. *Macromolecules* **2012**, *45* (23), 9475−9492.

(17) Doi, M.; Edwards, S. F. *The theory of polymer dynamics*; Clarendon Press: Oxford, U.K., 1986.

(18) Kremer, K.; Grest, G. S. Dynamics of Entangled Linear Polymer Melts: A Molecular-Dynamics Simulation. *J. Chem. Phys.* **1990**, *92* (8), 5057−5086.

(19) Muller-Plathe, F. Coarse-Graining in Polymer Simulation: From the Atomistic to the Mesoscopic Scale and Back. *ChemPhysChem* **2002**, *3* (9), 754−769.

(20) Müller-Plathe, F. Scale-Hopping in Computer Simulations of Polymers. *Soft Mater.* **2002**, *1* (1), 1−31.

(21) Reith, D.; Pütz, M.; Müller-Plathe, F. Deriving Effective Mesoscale Potentials from Atomistic Simulations. *J. Comput. Chem.* **2003**, *24* (13), 1624−1636.

(22) Spyriouni, T.; Tzoumanekas, C.; Theodorou, D.; Muller-Plathe, F.; Milano, G. Coarse-Grained and Reverse-Mapped United-Atom Simulations of Long-Chain Atactic Polystyrene Melts: Structure, Thermodynamic Properties, Chain Conformation, and Entanglements. *Macromolecules* **2007**, *40* (10), 3876−3885.

(23) Depa, P. K.; Maranas, J. K. Speed up of dynamic observables in coarse-grained molecular-dynamics simulations of unentangled polymers. *J. Chem. Phys.* **2005**, *123* (9), 094901−7.

(24) Tschöp, W.; Kremer, K.; Batoulis, J.; Bürger, T.; Hahn, O. Simulation of polymer melts. I. Coarse-graining procedure for polycarbonates. *Acta Polym.* **1998**, *49* (2−3), 61−74.

(25) Karimi-Varzaneh, H. A.; van der Vegt, N. F. A.; Müller-Plathe, F.; Carbone, P. How good are coarse-grained polymer models? A comparison for atactic polystyrene. *ChemPhysChem* **2012**, *13* (15), 3428−3439.

(26) Brini, E.; Algaer, E. A.; Ganguly, P.; Li, C.; Rodriguez-Ropero, F.; van der Vegt, N. F. A. Systematic Coarse-Graining Methods for Soft Matter Simulations - A Review. *Soft Matter* **2013**, *9* (7), 2108−2119.

(27) Milano, G.; Muller-Plathe, F. Mapping Atomistic Simulations to Mesoscopic Models: A Systematic Coarse-Graining Procedure for Vinyl Polymer Chains. *J. Phys. Chem. B* **2005**, *109* (39), 18609−18619.

(28) Harmandaris, V. A.; Adhikari, N. P.; van der Vegt, N. F. A.; Kremer, K. Hierarchical Modeling of Polystyrene: From Atomistic to Coarse-Grained Simulations. *Macromolecules* **2006**, *39* (19), 6708−6719.

(29) Sun, Q.; Faller, R. Systematic Coarse-Graining of a Polymer Blend: Polyisoprene and Polystyrene. *J. Chem. Theory Comput.* **2006**, *2* (3), 607−615.

(30) Huang, D. M.; Faller, R.; Do, K.; Moulé, A. J. Coarse-Grained Computer Simulations of Polymer/Fullerene Bulk Heterojunctions for Organic Photovoltaic Applications. *J. Chem. Theory Comput.* **2009**, *6* (2), 526−537.
(31) Izvekov, S.; Voth, G. A. Multiscale Coarse Graining of Liquid-State Systems. *J. Chem. Phys.* **2005**, *123* (13), 134105.
(32) Izvekov, S.; Voth, G. A. A Multiscale Coarse-Graining Method for Biomolecular Systems. *J. Phys. Chem. B* **2005**, *109* (7), 2469−2473.
(33) Hsu, D. D.; Xia, W.; Arturo, S. G.; Keten, S. Systematic Method for Thermomechanically Consistent Coarse-Graining: A Universal Model for Methacrylate-Based Polymers. *J. Chem. Theory Comput.* **2014**, *10* (6), 2514−2527.
(34) Agrawal, A.; Aryal, D.; Perahia, D.; Ge, T.; Grest, G. S. Coarse-Graining Atactic Polystyrene and Its Analogues. *Macromolecules* **2014**, *47* (9), 3210−3218.
(35) Maurel, G.; Schnell, B.; Goujon, F.; Couty, M.; Malfreyt, P. Multiscale Modeling Approach toward the Prediction of Viscoelastic Properties of Polymers. *J. Chem. Theory Comput.* **2012**, *8* (11), 4570−4579.
(36) Hezaveh, S.; Samanta, S.; De Nicola, A.; Milano, G.; Roccatano, D. Understanding the Interaction of Block Copolymers with DMPC Lipid Bilayer Using Coarse-Grained Molecular Dynamics Simulations. *J. Phys. Chem. B* **2012**, *116* (49), 14333−14345.
(37) Nawaz, S.; Carbone, P. Coarse-Graining Poly(ethylene oxide)−Poly(propylene oxide)−Poly(ethylene oxide) (PEO−PPO−PEO) Block Copolymers Using the MARTINI Force Field. *J. Phys. Chem. B* **2014**, *118* (6), 1648−1659.
(38) Huang, W.; Riniker, S.; van Gunsteren, W. F. Rapid Sampling of Folding Equilibria of β-Peptides in Methanol Using a Supramolecular Solvent Model. *J. Chem. Theory Comput.* **2014**, *10* (6), 2213−2223.
(39) Tschöp, W.; Kremer, K.; Hahn, O.; Batoulis, J.; Bürger, T. Simulation of Polymer Melts. II. From Coarse-Grained Models Back to Atomistic Description. *Acta Polym.* **1998**, *49* (2−3), 75−79.
(40) Ghanbari, A.; Ndoro, T. V. M; Leroy, F.; Rahimi, M.; Böhm, M. C.; Müller-Plathe, F. Interphase Structure in Silica−Polystyrene Nanocomposites: A Coarse-Grained Molecular Dynamics Study. *Macromolecules* **2011**, *45* (1), 572−584.
(41) Karimi-Varzaneh, H.; Müller-Plathe, F. Coarse-Grained Modeling for Macromolecular Chemistry. In *Multiscale Molecular Methods in Applied Chemistry*; Kirchner, B., Vrabec, J., Eds.; Springer: Berlin, Heidelberg, 2012; Vol. *307*, pp 295−321.
(42) Chen, X.; Carbone, P.; Santangelo, G.; Di Matteo, A.; Milano, G.; Muller-Plathe, F. Backmapping Coarse-Grained Polymer Models under Sheared Nonequilibrium Conditions. *Phys. Chem. Chem. Phys.* **2009**, *11* (12), 1977−1988.
(43) Santangelo, G.; Di Matteo, A.; Müller-Plathe, F.; Milano, G. From Mesoscale Back to Atomistic Models: A Fast Reverse-Mapping Procedure for Vinyl Polymer Chains. *J. Phys. Chem. B* **2007**, *111* (11), 2765−2773.
(44) De Nicola, A.; Milano, G.; Kawakatsu, T. A Hybrid Particle-Field Coarse-Grained Molecular Model for Pluronics Water Mixtures. *Macromol. Chem. Phys.* **2013**, *214* (17), 1940−1950.
(45) Peter, C.; Kremer, K. Multiscale Simulation of Soft Matter Systems - from the Atomistic to the Coarse-Grained Level and Back. *Soft Matter* **2009**, *5* (22), 4357−4366.
(46) Zhang, G.; Moreira, L. A.; Stuehn, T.; Daoulas, K. C.; Kremer, K. Equilibration of High Molecular Weight Polymer Melts: A Hierarchical Strategy. *ACS Macro Lett.* **2014**, *3* (2), 198−203.
(47) Laradji, M.; Guo, H.; Zuckermann, M. J. Off-Lattice Monte Carlo Simulation of Polymer Brushes in Good Solvents. *Phys. Rev. E* **1994**, *49* (4), 3199−3206.
(48) Khalatur, P. G. 1.16 - Molecular Dynamics Simulations in Polymer Science: Methods and Main Results. In *Polymer Science: A Comprehensive Reference*; Matyjaszewski, K., Möller, M., Eds.; Elsevier: Amsterdam, 2012; pp 417−460.
(49) Langner, K. M.; Sevink, G. J. A. Mesoscale Modeling of Block Copolymer Nanocomposites. *Soft Matter* **2012**, *8* (19), 5102−5118.
(50) Milano, G.; Kawakatsu, T.; De Nicola, A. A Hybrid Particle−Field Molecular Dynamics Approach: A Route toward Efficient Coarse-Grained Models for Biomembranes. *Phys. Biol.* **2013**, *10* (4), 045007.
(51) Daoulas, K. C.; Muller, M. Single Chain in Mean Field Simulations: Quasi-Instantaneous Field Approximation and Quantitative Comparison with Monte Carlo simulations. *J. Chem. Phys.* **2006**, *125* (18), 184904.
(52) Daoulas, K. C.; Muller, M.; de Pablo, J. J.; Nealey, P. F.; Smith, G. D. Morphology of Multi-Component Polymer Systems: Single Chain in Mean Field Simulation Studies. *Soft Matter* **2006**, *2* (7), 573−583.
(53) Stoykovich, M. P.; Muller, M.; Kim, S. O.; Solak, H. H.; Edwards, E. W.; de Pablo, J. J.; Nealey, P. F. Directed Assembly of Block Copolymer Blends into Nonregular Device-Oriented Structures. *Science* **2005**, *308* (5727), 1442.
(54) Ramírez-Hernández, A.; Suh, H. S.; Nealey, P. F.; de Pablo, J. J. Control of Directed Self-Assembly in Block Polymers by Polymeric Topcoats. *Macromolecules* **2014**, *47* (10), 3520−3527.
(55) De Nicola, A.; Zhao, Y.; Kawakatsu, T.; Roccatano, D.; Milano, G. Hybrid Particle-Field Coarse-Grained Models for Biological Phospholipids. *J. Chem. Theory Comput.* **2011**, *7*, 2947−2962.
(56) De Nicola, A.; Zhao, Y.; Kawakatsu, T.; Roccatano, D.; Milano, G. Validation of a Hybrid MD-SCF Coarse-Grained Model for DPPC in Non-Lamellar Phases. *Theor. Chem. Acc.* **2012**, *131* (3), 1167.
(57) Sarukhanyan, E.; De Nicola, A.; Roccatano, D.; Kawakatsu, T.; Milano, G. Spontaneous Insertion of Carbon Nanotube Bundles Inside Biomembranes: A Hybrid Particle-Field Coarse-Grained Molecular Dynamics Study. *Chem. Phys. Lett.* **2014**, *595*−*596* (0), 156−166.
(58) De Nicola, A.; Hezaveh, S.; Zhao, Y.; Kawakatsu, T.; Roccatano, D.; Milano, G. Micellar Drug Nanocarriers and Biomembranes: How Do They Interact? *Phys. Chem. Chem. Phys.* **2014**, *16*, 5093−5105.
(59) Sevink, G. J. A.; Charlaganov, M.; Fraaije, J. G. E. M. Coarse-Grained Hybrid Simulation of Liposomes. *Soft Matter* **2013**, *9* (10), 2816−2831.
(60) Milano, G.; Kawakatsu, T. Hybrid Particle-Field Molecular Dynamics Simulations for Dense Polymer Systems. *J. Chem. Phys.* **2009**, *130* (21), 214106.
(61) Milano, G.; Kawakatsu, T. Pressure Calculation in Hybrid Particle-Field Simulations. *J. Chem. Phys.* **2010**, *133* (21), 214102.
(62) Zhao, Y.; De Nicola, A.; Kawakatsu, T.; Milano, G. Hybrid Particle-Field Molecular Dynamics Simulations: Parallelization and Benchmarks. *J. Comput. Chem.* **2012**, *33* (8), 868−880.
(63) Hubbard, J. Calculation of Partition Functions. *Phys. Rev. Lett.* **1959**, *3* (2), 77−78.
(64) Chen, C.; Depa, P.; Maranas, J. K.; Garcia Sakai, V. Comparison of Explicit Atom, United Atom, and Coarse-Grained Simulations of Poly(methyl methacrylate). *J. Chem. Phys.* **2008**, *128* (12), 124906.
(65) Chen, C.; Maranas, J. K.; Garcia Sakai, V. Local Dynamics of Syndiotactic Poly(methyl methacrylate) Using Molecular Dynamics Simulation. *Macromolecules* **2006**, *39* (26), 9630−9640.
(66) Smith, G. D.; Borodin, O.; Bedrov, D. A Revised Quantum Chemistry-Based Potential for Poly(ethylene oxide) and Its Oligomers in Aqueous Solution. *J. Comput. Chem.* **2002**, *23* (15), 1480−1488.
(67) Chen, C.; Depa, P.; Sakai, V. G.; Maranas, J. K.; Lynn, J. W.; Peral, I.; Copley, J. R. D. A Comparison of United Atom, Explicit Atom, and Coarse-Grained Simulation Models for Poly(ethylene oxide). *J. Chem. Phys.* **2006**, *124* (23), 234901.
(68) Smith, G. D.; Yoon, D. Y.; Jaffe, R. L.; Colby, R. H.; Krishnamoorti, R.; Fetters, L. J. Conformations and Structures of Poly(oxyethylene) Melts from Molecular Dynamics Simulations and Small-Angle Neutron Scattering Experiments. *Macromolecules* **1996**, *29* (10), 3462−3469.
(69) Andersen, H. C. Molecular Dynamics Simulations at Constant Pressure and/or Temperature. *J. Chem. Phys.* **1980**, *72* (4), 2384−2393.
(70) Berendsen, H. J. C.; Postma, J. P. M.; van Gunsteren, W. F.; Di Nola, A.; Haak, J. R. Molecular Dynamics with Coupling to an External bath. *J. Chem. Phys.* **1984**, *81* (8), 3684−3690.
(71) Allen, M. P.; Tildesley, D. J. *Computer Simulation of Liquids*; Clarendon Press: Oxford, 1987.

(72) Brandrup, J.; Immergut, E. H. *Polymer Handbook*, 3rd ed. ed.; John Wiley & Sons: New York, 1989.
(73) Karol, M. More Data about Dielectric and Electret Properties of Poly(methyl methacrylate). *J. Phys. D: Appl. Phys.* **1997**, *30* (9), 1383.
(74) Frenkel, D.; Smit, B. *Understanding Molecular Simulations. From Algorithm to Applications*; Academic Press: San Diego, 2002.
(75) Brown, D.; Clarke, J. H. R.; Okuda, M.; Yamazaki, T. The Preparation of Polymer Melt Samples for Computer Simulation Studies. *J. Chem. Phys.* **1994**, *100* (8), 6011−6018.
(76) Fujii, Y.; Tamai, Y.; Konishi, T.; Yamakawa, H. Intrinsic Viscosity of Oligo- and Poly(methyl methacrylate)s. *Macromolecules* **1991**, *24* (7), 1608−1614.
(77) O'Reilly, J. M.; Teegarden, D. M.; Wignall, G. D. Small- and Intermediate-Angle Neutron Scattering from Stereoregular Poly(methyl methacrylate). *Macromolecules* **1985**, *18* (12), 2747−2752.
(78) Krishnamoorti, R.; Graessley, W. W.; Zirkel, A.; Richter, D.; Hadjichristidis, N.; Fetters, L. J.; Lohse, D. J. Melt-State Polymer Chain Dimensions As a Function of Temperature. *J. Polym. Sci., Part B: Polym. Phys.* **2002**, *40* (16), 1768−1776.
(79) Flory, P. J. Foundations of Rotational Isomeric State Theory and General Methods for Generating Configurational Averages. *Macromolecules* **1974**, *7* (3), 381−392.
(80) Yoon, D. Y.; Suter, U. W.; Sundararajan, P. R.; Flory, P. J. Conformational Characteristics of Poly(methyl acrylate). *Macromolecules* **1975**, *8* (6), 784−789.
(81) Crissman, J. M.; McKenna, G. B. Physical and Chemical Aging in PMMA and Their Effects on Creep and Creep Rupture Behavior. *J. Polym. Sci., Part B: Polym. Phys.* **1990**, *28*, 1463−1473.
(82) Müller, M.; Daoulas, K. C. Calculating the Free Energy of Self-Assembled Structures by Thermodynamic Integration. *J. Chem. Phys.* **2008**, *128* (2), 024903.
(83) Windle, A. H. X-ray Scattering Measurements of Order in Non-Crystalline Polymers. *Pure Appl. Chem.* **1985**, *57* (11), 1627−1639.
(84) Sides, S. W.; Kim, B. J.; Kramer, E. J.; Fredrickson, G. H. Hybrid Particle-Field Simulations of Polymer Nanocomposites. *Phys. Rev. Lett.* **2006**, *96* (25), 250601.